# Human Mitochondrial Manganese Superoxide Dismutase Polymorphic Variant Ile58Thr Reduces Activity by Destabilizing the Tetrameric Interface[†,‡]

Gloria E. O. Borgstahl,[§] Hans E. Parge,[§,||] Michael J. Hickey,[§] Michael J. Johnson,[§] Maurice Boissinot,[§,⊥] Robert A. Hallewell,[#] James R. Lepock,[○] Diane E. Cabelli,[▽] and John A. Tainer*[,§]

*Department of Molecular Biology, The Scripps Research Institute, La Jolla, California 92037, Department of Biochemistry, Imperial College, London SW7 2AZ, U.K., Department of Physics, University of Waterloo, Waterloo, Ontario N2L3G1, Canada, and Department of Chemistry, Brookhaven National Laboratory, Upton, New York 11973*

*Received August 11, 1995; Revised Manuscript Received December 20, 1995*[⊗]

ABSTRACT: Human manganese superoxide dismutase (MnSOD) is a homotetrameric enzyme which protects mitochondria against oxygen-mediated free radical damage. Within each subunit, both the N-terminal helical hairpin and C-terminal $\alpha/\beta$ domains contribute ligands to the catalytic manganese site. Two identical four-helix bundles, symmetrically assembled from the N-terminal helical hairpins, form a novel tetrameric interface that stabilizes the active sites. The 2.5 Å crystallographic structure of the naturally occurring polymorphic variant Ile58Thr MnSOD reveals that the helical hairpin mutation Thr58 causes two packing defects in each of the two four-helix bundles of the tetrameric interface. Similar mutations, expected to cause packing defects in the Cu,ZnSOD dimer interface, are associated with the degenerative disease amyotrophic lateral sclerosis. Ile58Thr MnSOD is primarily dimeric in solution and is significantly less thermostable than the normal enzyme, with decreases of 15 °C in the main melting temperature and 20 °C in the heat-inactivation temperature. Consequently, this mutant MnSOD is compromised at normal body temperatures: thermal inactivation, predicted from the decrease in thermal stability, occurs with a theoretical half-life of only 3.2 h at 37 °C (1.4 h at 41 °C), compared with 3.1 years for native MnSOD. This prediction is supported by direct measurements: incubation at 41.7 °C for 3 h has no effect on the activity of native MnSOD but completely inactivates mutant MnSOD. Rapid inactivation of Ile58Thr MnSOD at the elevated temperatures associated with fever and inflammation could provide an early advantage by killing infected cells, but also would increase superoxide-mediated oxidative damage and perhaps contribute to late-onset diseases.

Superoxide dismutases (SODs)[1] defend cells against oxidative damage and control superoxide concentrations. Superoxide is produced in many biological reactions, for example, oxidative phosphorylation, and can oxidatively damage DNA and inactivate enzymes (Fridovich, 1986; Halliwell & Gutteridge, 1989). Because oxygen scavenges most other radicals to form superoxide, SODs play a pivotal role in controlling reactive oxygen and other radical species in cells (Winterbourn, 1993), which can act as cellular messengers (Khan & Wilson, 1995). SODs dismute two molecules of superoxide anion to form hydrogen peroxide and molecular oxygen. Humans have three isoenzymes of superoxide dismutase: dimeric, cytoplasmic Cu,ZnSOD (Fridovich, 1986); tetrameric, mitochondrial MnSOD (Ho & Crapo, 1988; Beyer et al., 1991); and tetrameric, extracellular Cu,ZnSOD (Hjalmarsson et al., 1987). Mitochondria are particularly prone to oxidative DNA damage because they metabolize over 95% of the cell's oxygen (Chance et al., 1979; Guidot et al., 1993) but lack histones and have poor DNA repair (Richter et al., 1988). Within mitochondria, MnSOD is the primary defense against reactive oxygen, and as mitochondrial defects are associated with the degenerative diseases of aging (Ames et al., 1993), MnSOD may play a key defensive role against late-onset diseases.

Defects in SOD contribute to neurodegenerative diseases apparently through the breakdown of free radical defense mechanisms. Point mutations in the Cu,ZnSOD gene (SOD1) occur in patients with the fatal neurodegenerative disorder familial amyotrophic lateral sclerosis (ALS) (Deng et al., 1993). Preliminary reports associate polymorphisms in the MnSOD gene with Parkinson's disease (Eggers et al., 1994) and find low MnSOD levels in the skeletal muscle and serum of patients with Duchenne muscular dystrophy (MD), congenital MD, ALS, Charcot−Marie−Tooth disease, and Kennedy−Alter−Sung syndrome (Yahara et al., 1991). Therefore, MnSOD defects may contribute to neurodegenerative diseases.

[†] This work was supported by NIH Grant GM48495 (J.A.T. and R.A.H.), NIH Grant GM23658 (D.E.C.), the Natural Sciences and Engineering Research Council of Canada (J.R.L.), Welcome Trust Grant 038968 (R.A.H.), and fellowships from FRSQ and MRC Canada (M.B.).

[‡] Crystallographic coordinates were deposited in the Brookhaven Protein Data Bank (code 1VAR).

* Author to whom correspondence should be addressed: phone, (619) 554-8119; email, jat@scripps.edu.

[§] The Scripps Research Institute.

[||] Present address: Research Laboratories, Agouron Pharmaceuticals, Inc., 3565 General Atomics Court, San Diego, CA 92121.

[⊥] Present address: Department of Microbiology, Laval University, Quebec G1K 7P4, Canada.

[#] Imperial College.

[○] University of Waterloo.

[▽] Brookhaven National Laboratory.

[⊗] Abstract published in *Advance ACS Abstracts,* February 15, 1996.

[1] Abbreviations: SOD, superoxide dismutase; ALS, amyotrophic lateral sclerosis; MW, molecular weight; EDTA, ethylenediaminetetraacetic acid; MD, muscular dystrophy; RFLP, restriction fragment length polymorphism; DSC, differential scanning calorimetry; GFC, gel filtration chromatography; SOD1, gene encoding human Cu,ZnSOD; SOD2, gene encoding human mitochondrial MnSOD.

0006-2960/96/0435-4287$12.00/0 

The degenerative disease diabetes is also associated with oxidative damage (Malaisse et al., 1982; Crouch et al., 1981) and linked to defects in SOD. In humans, a restriction fragment length polymorphism (RFLP) of the MnSOD gene (*SOD2*) is linked to type I diabetes (Davies et al., 1994), and MnSOD with decreased activity is found in the leukocytes of diabetics (Nath et al., 1984). In diabetic animals, Cu,ZnSOD is protective of healthy pancreatic islet tissue transplants (Nomikos et al., 1989), and MnSOD defects could explain the sensitivity of pancreatic $\beta$-cells to oxygen free radical damage.

In humans, oxidative stress from ionizing radiation, chemotherapeutic drugs, and environmental toxins induces MnSOD gene expression, but this protective induction decreases sharply with age (Niwa et al., 1993). Mediators of oxidative stress, including tumor necrosis factor-$\alpha$ (TNF), interleukin 1, lipopolysaccharides, and phorbol esters, also induce MnSOD (Masuda et al., 1988; Wong & Goeddel, 1988). MnSOD is essential for cellular resistance to TNF cytotoxicity (Wong et al., 1989). MnSOD gene expression suppresses tumors (St. Clair et al., 1992; Church et al., 1993), perhaps by decreasing reactive oxygen species that promote cancer (Oberley & Beuttner, 1979; Cerutti, 1985; Wong et al., 1989). Downregulation of MnSOD gene expression after immortalization and transformation of mouse liver cells (Sun et al., 1993) indicates that the decreased MnSOD activity in tumors (Oberley & Beuttner, 1979; Sun, 1990) is due to decreased amounts of enzyme. Melanoma cells frequently lose the region of chromosome 6 that contains the SOD2 gene (Millikin et al., 1991), and introduction of a normal chromosome 6 into human melanoma cell lines suppresses tumorigenicity (Trent et al., 1990). Furthermore, overexpression of MnSOD suppresses radiation-induced neoplastic transformation in mouse embryonic fibroblasts (St. Clair et al., 1992) and the malignant phenotype of human melanoma cells (Church et al., 1993). Thus, MnSOD suppresses carcinogenesis.

Just as defects in Cu,ZnSOD contribute to ALS, defects in MnSOD may contribute to degenerative diseases such as Parkinson's disease, MD, diabetes, and cancer. Here, we determine and analyze the assembly state, crystallographic structure, stability, and activity of a naturally occurring, single-site, human polymorphic variant of MnSOD. The Ile58Thr point mutation (Ho & Crapo, 1988; Wispe et al., 1989) is located in the heart of the four-helix bundle tetrameric interface of the native enzyme (Borgstahl et al., 1992), making Ile58Thr MnSOD a prototype for polymorphic variants that destabilize the human MnSOD tetramer. The crystallographic structure of Ile58Thr MnSOD reveals the structural defects in this variant that are responsible for its tetrameric disassembly, decreased thermostability, and increased thermal inactivation.

## METHODS

*Expression and Purification.* The Ile58Thr MnSOD mutant was made by a modified Kunkel mutagenesis (Kunkel et al., 1987) of the native MnSOD gene (Borgstahl et al., 1992). The native MnSOD gene (SOD2) was cloned into pBluescriptIIKS$^+$ (Stratagene) and transfected into the CJ236 strain of *Escherichia coli* which is *dut*$^-$*ung*$^-$. Single-stranded DNA was purified from cells superinfected with VCSM13 helper phage. Double-stranded DNA, made from this single-stranded DNA template plus a 20-base oligonucleotide containing the Thr58 mutation, was transfected into XL1-Blue *E. coli* (*dut*$^+$*ung*$^+$; Stratagene) under ampicillin selection. Mini DNA preps were done and four clones sequenced. A clone with the Ile58Thr mutation was subcloned into the expression vector, and *sodAsodB E. coli* which lack MnSOD and FeSOD were transformed, cultured, and induced as previously described (Hallewell et al., 1985). The mutant protein was purified following the protocol for native MnSOD (Borgstahl et al., 1992) except that the yield was substantially lower because the mutant protein was less stable and precipitated easily.

*Gel Filtration Chromatography*. Purified native and mutant MnSOD and *E. coli* FeSOD dimer (Sigma) samples were loaded onto a Superose 12, HR 10/30 (Pharmacia) column, separated by FPLC (Pharmacia) at 4 °C, and protein peaks were detected by UV spectrometry. Four molecular weight standards were used to estimate molecular weights: 158 000 $\gamma$-globulin, 44 000 ovalbumin, and 17 500 myoglobin (Pharmacia standards) plus 88 000 native human MnSOD (20 mg/mL, 250 $\mu$g total).

*Crystallization and Diffraction Data Collection.* Crystals of recombinant human MnSOD Ile58Thr were grown at room temperature using the hanging drop method. The best crystals grew from solutions consisting of 10 mg/mL protein buffered in 50 mM phosphate, pH 7.8, and 19% PEG 4000. Crystals are isomorphous with native crystals (Borgstahl et al., 1992), belonging to the space group $P2_12_12$ with cell dimensions $a = 75.0$ Å, $b = 78.1$ Å, and $c = 68.1$ Å and one dimer per asymmetric unit.

Data were collected from one crystal with a Mar Research image plate area detector at Stanford Synchrotron Radiation Laboratory (SSRL) and processed using the MOSFLM program suite (Leslie et al., 1986). A total of 13 540 unique reflections (72 924 total measurements) were collected. These data are 95% complete from 10 to 2.5 Å resolution [87% when a signal-to-noise ratio ($I/\sigma I$) greater than 3 is applied] and 95% complete for the 2.6−2.5 Å resolution shell (75% complete with a $3\sigma$ cutoff). The $R_{sym}$ on intensities was 11.8%.

*Crystallographic Refinement*. The atomic model was refined with X-PLOR (Brünger et al., 1990). The molecular graphics programs TOM (Jones, 1985) and Xfit (McRee, 1992) were used for electron density map display and fitting. $F_o - F_c$ omit electron density maps were made by omitting atoms from the model (<10%) and refining the protein coordinates by simulated annealing before calculating structure factor amplitudes and phases.

*Differential Scanning Calorimetry*. A Microcal-2 high-sensitivity differential scanning calorimeter was used to obtain all denaturation profiles. MnSOD at 2.4−3.2 mg/mL in 2 mM potassium phosphate buffer (pH 7.8) was deaerated under mild vacuum for 5 min and immediately scanned at a rate of temperature increase of 1 °C/min. The baseline and change in specific heat ($\Delta C_p$) upon denaturation were corrected as previously described (Lepock et al., 1990b). To check for reversibility of the main transitions, partial scans were made to 75 °C for the native enzyme and 45 and 65 °C for the mutant enzyme.

The two peaks of the DSC profiles were deconvoluted using both a reversible and a two-state irreversible model (Sturtevant, 1987; McRee et al., 1990). The latter model

requires the assumptions that each peak represents an irreversible, one-step transition of the form native → denatured, obeying pseudo-first-order kinetics, and that the temperature dependence of the rate constant for denaturation obeys the Arrhenius relation. Thus:

$$\frac{df_D(t)}{dt} = k(T)[1 - f_D(t)] \quad (1)$$

$$k(T) = e^{A - E_A/RT} \quad (2)$$

where $f_D$ is the fraction denatured, $t$ is the elapsed time, $k$ is the rate constant for denaturation, $T$ is the absolute temperature, $A$ is the pre-exponential or frequency factor, $E_A$ is the activation energy giving the temperature dependence of $k$, and $R$ is the gas constant. During a DSC scan, temperature increases uniformly with time ($t$):

$$T(t) = T_0 + \upsilon t \quad (3)$$

where $T_0$ is the initial temperature and $\upsilon$ the scan rate. Combining these equations gives

$$\frac{df_D[T(t)]}{dt} = e^{A - E_A/R(T_0 + \upsilon t)}(1 - f_D[T(t)]) \quad (4)$$

which can be solved for $f_D$ as a function of temperature. The apparent excess specific heat during the transition is given by

$$C_p^{ex}(T) = \Delta H_c\left(\frac{df_D}{dT}\right) \quad (5)$$

where $\Delta H_c$ is the apparent calorimetric enthalpy. The best fits for $E_A$, $A$, and $\Delta H_c$ for each peak, assuming irreversible denaturation, were obtained using the simplex, nonlinear curve-fitting algorithm (Lepock et al., 1990a,b). The algorithm proposed by Freire and Biltonen (1978) and modified by Filimonov et al. (1982) was used for curve fitting and deconvolution assuming reversible denaturation. The fits were refined using the simplex algorithm to obtain $\Delta H$, $\Delta S$, and $T_m$, defined as the temperature of half-completion, for each transition.

*Activity Measurements*. Superoxide dismutation reaction rates of Ile58Thr and native MnSOD were measured in pulse radiolytic experiments carried out with the 2 MeV van der Graaff accelerator at Brookhaven National Laboratory as described previously (Cabelli & Bielski, 1983). Superoxide radicals were generated in air/oxygen-saturated aqueous solutions (Schwarz, 1981) containing 10 mM sodium formate. The water was purified with a Millipore ultrapurification system. Any adventitious metal ions in solution were scavenged by the addition of 20−60 $\mu$M ethylenediaminetetraacetic acid (EDTA). Solutions were buffered with 5−10 mM sodium dihydrogen phosphate. The decay of superoxide radical was followed spectrophotometrically at 245−270 nm.

Low substrate/enzyme ratios (<5/1) yielded data that could be fit with a simple unimolecular decay. Catalytic rate measurements were made assuming the mechanism (McAdam et al., 1977):

$$Mn^{3+}SOD + O_2^{\bullet -} \rightleftharpoons Mn^{2+}SOD + O_2 \quad (6)$$

$$Mn^{2+}SOD + O_2^{\bullet -} + 2H^+ \rightleftharpoons Mn^{3+}SOD + H_2O_2 \quad (7)$$

$$Mn^{2+}SOD + O_2^{\bullet -} \rightleftharpoons MnO_2^{\bullet -}SOD \quad (8)$$

$$MnO_2^{\bullet -}SOD + 2H^+ \rightleftharpoons Mn^{3+}SOD + H_2O_2 \quad (9)$$

Reactions 6 and 7 in this mechanism describe the catalytic disproportionation of superoxide and involve the reduction and subsequent reoxidation of the metal. This is analogous to the well-established mechanism in Cu,ZnSOD where $Cu^{2+}$ is the initial state of the enzyme. The rate constants quoted here are for reactions 6 and 7 (observed to be roughly equivalent). The cycle described by reactions 6, 8, and 9 is observed only at a much higher substrate/enzyme ratio.

Atomic absorption spectroscopy (Pye-Unicom or GBC instrument) was used to determine the concentration of manganese in the sample. Studies were carried out generating 1−20 $\mu$M $O_2^{\bullet -}$ using 0.05−5 $\mu$M enzyme. The rate constants are reported here relative to the enzyme concentration, assuming that the native enzyme is a tetramer and the Ile58Thr mutant is a dimer.

Rates of irreversible thermal inactivation were measured for native and mutant MnSOD. Samples (pH 7.48, 0.214 $\mu$M manganese, 10 mM formate, 10 mM phosphate, and 20 $\mu$M EDTA, in air) were heated to 41.7 °C for 3 h, cooled, and tested for residual activity. The temperature dependence of MnSOD reaction rate (Figure 7) was measured at pH 7.89, 2.14 $\mu$M manganese, 10 mM formate, 5 mM phosphate, and 60 $\mu$M EDTA, in air. The sample was studied from 25 to 56 °C and was changed every 5 min.

## RESULTS

*Subunit Association*. Native human mitochondrial MnSOD is a homotetramer composed of four identical 198-residue subunits and assembled about three, orthogonal 2-fold axes of symmetry (Borgstahl et al., 1992). Two monomers are joined by a dimeric interface, named for its similarity to the dimeric bacterial SODs, to form dimers. A tetrameric interface, mainly composed of two four-helix bundles, joins two dimers to form a tetramer.

The unusual characteristics of Ile58Thr MnSOD were first detected during protein purification. Purification of the mutant protein was more difficult than native because it precipitated easily, and due to this instability it could not be concentrated to greater than 6.3 mg/mL. Also during gel filtration chromatography (GFC), the mutant MnSOD had unusual properties. Native MnSOD tetramer elutes as a single sharp peak with the expected molecular weight (MW) of 88 000 (Figure 1A), and the peak position and sharpness do not change with increased protein concentration (data not shown). On the other hand, the mutant MnSOD elutes with a lower than expected mass, and its apparent MW is dependent on protein concentration. At 20 $\mu$g/mL (Figure 1B), the mutant MnSOD elutes as a sharp peak with an apparent MW of 46 000, and when concentrated to 6.3 mg/mL (Figure 1C) the elution peak broadens and is centered at 54 000. All fractions from mutant MnSOD GFC peaks ran as 22 000 MnSOD monomers on SDS−PAGE.

The smaller size of mutant MnSOD on GFC suggests the increased concentration of a dimeric form of Ile58Thr MnSOD over the normal tetrameric form. A dimeric form was not observed for native MnSOD, even when it was diluted to 200 $\mu$g/mL (Figure 1A). Mutant MnSOD has an elution position that is similar to that of dimeric bacterial

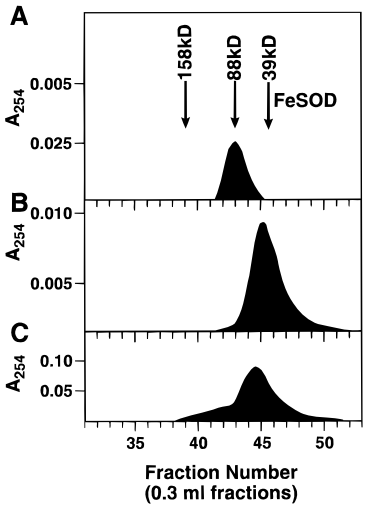


FIGURE 1: Gel filtration chromatography of purified native and mutant MnSOD. (A) Native MnSOD at 200 $\mu$g/mL (40 $\mu$g total) elutes with apparent MW of 88 000, (B) Mutant Ile58Thr MnSOD at 200 $\mu$g/mL (40 $\mu$g total) elutes with apparent MW of 46 000. (C) Mutant Ile58Thr MnSOD at 6.3 mg/mL (250 $\mu$g total) elutes as a broad peak centered at 54 000. The elution positions of the maximum peak heights for the 39 000 *E. coli* FeSOD dimer (6.3 mg/mL, 250 $\mu$g total) and the 158 000 and 88 000 standards are indicated with arrows at the top.

FeSOD (Figure 1B). The broad GFC peak at higher concentration for mutant MnSOD (Figure 1C) suggests a mixture of an elongated, dimeric form plus a higher aggregation form. The existence of a higher aggregation state for mutant MnSOD (Figure 1C) suggests a fast equilibrium for some of the material between a dimeric and tetrameric form. The absence of a tetrameric form of approximately 88 000 for mutant MnSOD (Figure 1B,C) suggests that the Ile58Thr mutation destabilizes the tetrameric interface and favors a predominantly dimeric form in solution.

*Structure Determination and Quality*. Although Ile58Thr MnSOD is apparently predominantly dimeric and a mixed dimer−tetramer equilibrium in solution, the high protein concentration and added precipitant required for crystallization drove the dimer−tetramer equilibrium to the tetramer and gave crystals with the same symmetry relationships as native MnSOD crystals (Borgstahl et al., 1992). The crystallographic asymmetric unit is a dimer, and a crystallographic 2-fold axis of symmetry forms the homotetramer (Figure 3B).

The difference electron density map (Figure 2A) shows negative (red) electron density at Ile58 indicating the removal of the $C^{\delta}$ atom, positive (blue) density at Thr58 indicating a shift in the side-chain position for residue 58, and additional difference peaks throughout the tetrameric interface (not shown). These significant structural differences yielded an *R*-value of 42% between the native model and the mutant diffraction data (for data between 10 and 3 Å resolution), which was reduced to 28.1% by rigid body refinement of the two native MnSOD subunits relative to each other (with residue 58 modeled as Ala). Two rounds of conventional refinement, including data with a signal-to-noise ratio ($I/\sigma I$) better than 3 from 10 to 2.5 Å resolution, resulted in an *R*-value of 22.4%. The Thr58 side chain was added and fit to omit $F_o - F_c$ Fourier maps. Omit electron density of mutant (Figure 2B) and native MnSOD (Figure 2C) clearly distinguishes mutant Thr58 from native Ile58. Temperature factor (*B*-value) refinement reduced the *R*-value to 20.8%. Finally, water molecules with electron density greater than $3\sigma$ were included in the atomic model and refined.

The atomic model of Ile58Thr MnSOD, consisting of 3144 non-hydrogen protein atoms, 2 manganese atoms, and 175 water molecules, has an *R*-value of 17.0% with excellent stereochemistry. The overall deviations from ideal geometry were 0.015 Å for bond distances and 1.86° for bond angles. The Ile58Thr MnSOD structures have an average *B*-value of 28.0 Å$^2$ for protein atoms, compared to 23.9 Å$^2$ for the native structure after similar refinement at 2.5 Å resolution. The lower *B*-values of the native enzyme reflect mainly the higher quality of the native data at 2.5 Å resolution (crystals diffracted to 2.2 Å resolution) and possibly lower thermal motion of the native enzyme relative to the mutant enzyme. The average *B*-value of water molecules included in the Ile58Thr MnSOD structure was 39.7 Å$^2$ (standard deviation = 11.1) with a minimum of 11.3 Å$^2$ and a maximum of 59.3 Å$^2$. The main-chain dihedral angles ($\phi$ and $\psi$) and the side-chain torsion angle $\chi 1$ are very similar for Ile58 (average $\phi = -77°$, $\psi = -34°$, and $\chi 1 = -70°$) and Thr58 (average $\phi = -68°$, $\psi = -46°$, and $\chi 1 = -70°$).

*Atomic Structures*. Ile58Thr MnSOD has the same overall structure as native MnSOD. The RMS deviation after superposition of a native MnSOD subunit onto an Ile58Thr MnSOD subunit is only 0.35 Å (main chain only). The MnSOD subunit fold can be divided into two distinct domains: a N-terminal helical hairpin domain (residues 1−84) and a C-terminal $\alpha/\beta$ domain (residues 85−198; Figure 3A). The active site manganese joins these two domains. The Ile58Thr mutation is located at the N-terminal end of helix $\alpha 2$ of the helical hairpin (Figure 3A), which contributes manganese ligand His74 to the active site. Two-fold symmetry places two copies of the single-site mutation Ile58Thr in each four-helix bundle, and two four-helix bundles form the tetrameric interface (Figure 3B). Thus, the effect of the single amino acid mutation is quadrupled in the assembled tetrameric enzyme.

In each mutant four-helix bundle, 30 Å$^2$ more surface area is buried between the helical hairpins, with the native and mutant burying 820 and 850 Å$^2$, respectively. In the native tetrameric interface, hydrophobic residue Ile58 is the largest contributor of buried surface area (75 Å$^2$, 1.6 Å probe), with eight intersubunit van der Waals (VDW) contacts within 4 Å (Figure 4A). Ile58 has VDW contacts with residues Leu64 (atoms O and $C^{\delta 2}$), Lys65 ($C^{\alpha}$, $C^{\delta}$, and $C^{\gamma}$), Gly69 (N), and Pro145 ($C^{\delta}$ and $C^{\gamma}$). In the mutant interface, Thr58 contributes only 56 Å$^2$ to the interface and partly maintains intersubunit VDW contacts with Pro145 ($C^{\gamma}$) and Lys65 ($C^{\delta}$), gains contacts with Gly148 ($C^{\alpha}$, C, and O), and completely loses interactions with residues 64 and 69. Interestingly, Thr58 $O^{\gamma 1}$ forms an intrasubunit hydrogen bond with the carbonyl oxygen of Val54 (Figure 4A), a common hydrogen-bonding pattern for helical Thr residues (Gray & Matthews, 1984).

Overall, the quaternary structure is conserved between the mutant and native enzyme, but the mutant interface has shifted in compensation for the loss of a methyl group (Figure 4B). Replacing the native Ile58 side chain with Thr results in the concerted movement of residues across the interface from Thr58 toward the vacated space. The $C^{\alpha}$ atoms of

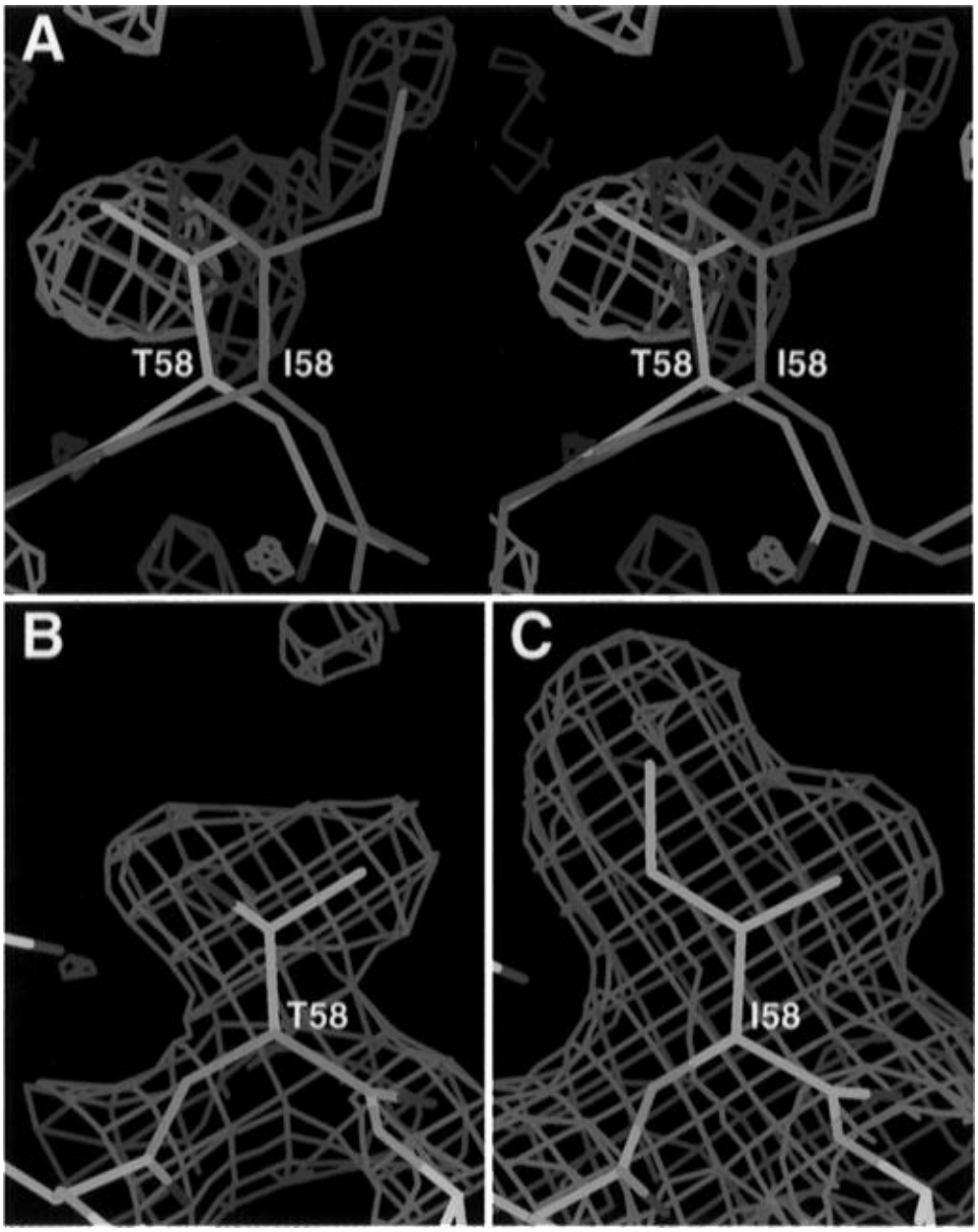


FIGURE 2: Electron density and refined atomic structures of native and mutant Ile58Thr MnSOD. (A) Stereo pair of the difference electron density map calculated by subtracting mutant diffraction amplitudes from native diffraction amplitudes ($F_{nat} - F_{mut}$) and phased with native MnSOD phases ($2\sigma$ contours; colored positive blue and negative red). Ile58 bonds of native MnSOD (Brookhaven Protein Data Bank entry 1ABM) are in green, and Thr58 has atom colors of carbon in yellow, oxygen in red, and nitrogen in blue. Omit $F_o - F_c$ electron density for (B) Ile58 of native MnSOD (10−2.2 Å resolution) and (C) Thr58 from mutant MnSOD (10−2.5 Å resolution) where the tripeptide 57−59 was left out of the phase calculation. Part A is rotated 180° relative to parts B and C.

residues 65−69 shift 0.4−0.6 Å, and residues 142−149 shift 0.4−0.8 Å. The movement of surrounding residues to fill a hole is typical of proteins with a cavity-creating mutation (McRee et al., 1990; Eriksson et al., 1992).

The concerted movement of the tetrameric interface surrounding Thr58 does not completely fill the gap, and packing defects remain in the mutant interface, explaining the lower stability despite the increased buried surface area (Figure 5). The native Ile58 side chain fits perfectly into the interface shape (Figure 5A), producing a very stable tetrameric enzyme. Yet, the Thr58 mutation fits poorly and leaves a significant cavity (∼1.5 Å diameter) in the interface (Figure 5B). There are two such cavities per four-helix bundle (note packing defects at the top and bottom of Figure 5B) and four per MnSOD tetramer (Figure 3B). These packing defects disrupt the dimer−tetramer equilibrium and favor the dimer over the tetramer in solution as found experimentally (Figure 1).

*Thermal Stability*. This disruption of the MnSOD tetramer, involving the helical hairpin that provides two manganese ligands, causes an overall reduction of stability and activity. The thermal stability of native and Ile58Thr MnSOD was determined by differential scanning calorimetry (DSC). Two peaks are observed for native MnSOD (Figure 6A), a small one (labeled B) with $T_m$ ∼68 °C and a much larger one (labeled C) with $T_m$ ∼88 °C. The $T_m$'s for peaks B and C for Ile58Thr MnSOD are decreased 13 and 16 °C relative to native MnSOD, respectively (Figure 6B). Peak C is sharper for the mutant than the native, possibly because of a weak exotherm at 75−80 °C in the mutant. Exotherms following denaturation are generally due to protein aggregation. The apparent calorimetric enthalpy of transition C (1.2

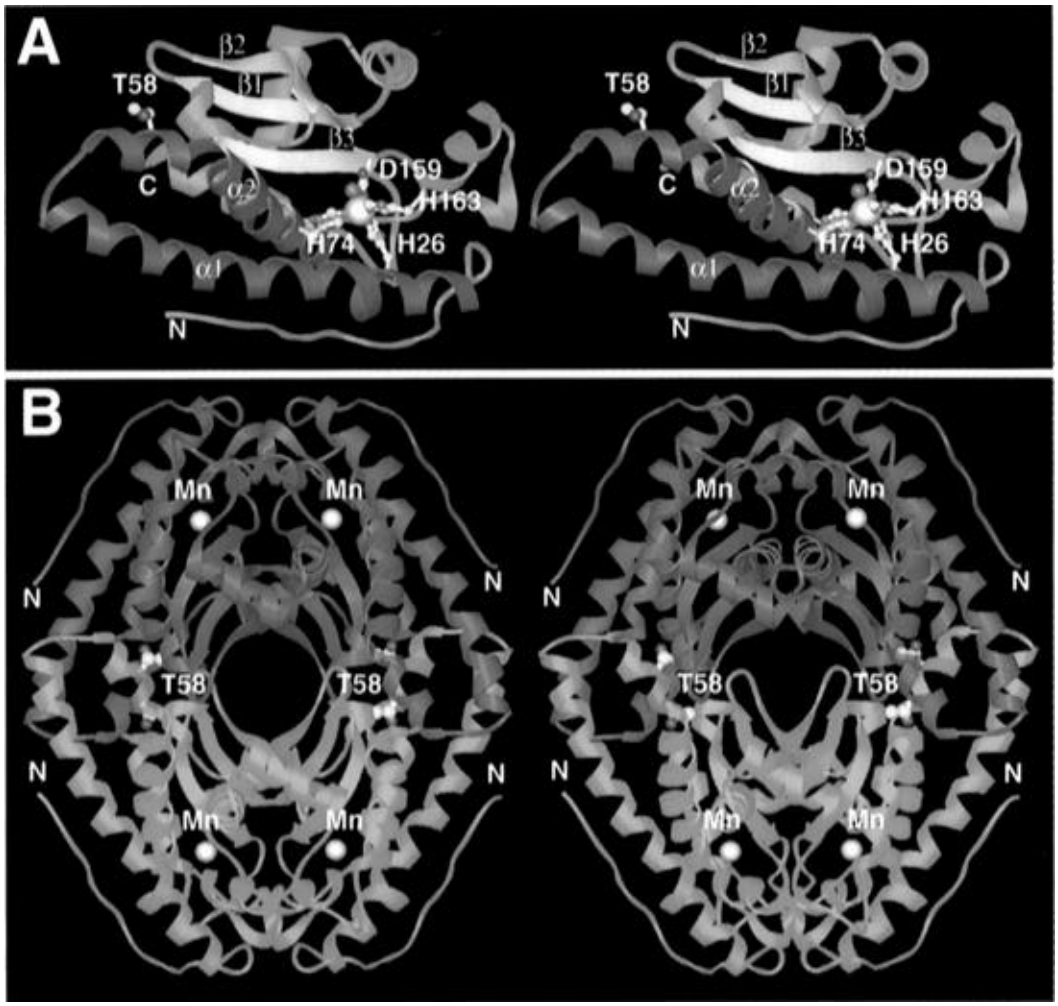


FIGURE 3: Stereo RIBBONS (Carson, 1991) diagrams of the topological location of the Ile58Thr mutation on human mitochondrial MnSOD. (A) A single MnSOD subunit. The N-terminal domain (bottom) is made up of the blue N-terminal loop and two long magenta α-helices (α1 and α2). The Ile58Thr mutation is located on α2 of the helical hairpin. The C-terminal α/*β* domain (top) is composed of five blue α-helices and three yellow *β*-strands. Residues His26 and His74 from the N-terminal domain and Asp159 and His163 from the C-terminal domain ligate the active site manganese (pink sphere). The fifth ligand is a water molecule (blue sphere). The manganese atom and mutation site are 26.5 Å apart. (B) The MnSOD homotetramer. The A/B (magenta, top) and C/D (blue, bottom) dimers each form a crystallographic asymmetric unit, and dimer interfaces form vertically across the top and bottom. The tetrameric interface forms around the crystallographic 2-fold axis along the horizontal (*c* axis) and joins the magenta and blue dimers with two four-helix bundles. The Ile58Thr mutation is located in the tetrameric four-helix bundle interface. The four Thr58 side chains have yellow (carbon) and red (oxygen) spheres (center right and center left).

cal/g) is in the range of the enthalpy of denaturation for other proteins, suggesting that transition C is the main unfolding transition of MnSOD. Transition B has a much lower enthalpy (0.17 cal/g), but activity measurements as a function of temperature (see below) show that this pre-unfolding transition is responsible for thermal inactivation. The mutant has a very low temperature transition (Figure 6B; peak A, $T_m$ ~34 °C) that is not present in native MnSOD.

Partial scans to the end of each transition determined that all transitions are highly irreversible (results not shown). Thus, the DSC data were fit (Figure 6A,B) using an irreversible, two-state model. The variable parameters are the Arrhenius constants, $E_A$ and $A$, which can then be used to calculate rates of inactivation (Table 1, for transition B). The predicted rates of inactivation at 37 °C, assuming that inactivation is due to transition B, are $7.0 \times 10^{-9}$ and $0.5 \times 10^{-4}$ $s^{-1}$ for the native and mutant, respectively. These correspond to half-times of inactivation of 3.1 years and 3.2 h, respectively. At 41 °C, the predicted rate of inactivation for the mutant is $1.4 \times 10^{-4}$ $s^{-1}$, which corresponds to a half-time of inactivation of only 1.4 h.

The estimated destabilization of the mutant, given as $\Delta\Delta G$, was calculated from the thermodynamic parameters obtained assuming reversible transitions (Table 2). A reversible analysis of an apparently irreversible process is appropriate, and is commonly done, if there is little accumulation of the irreversibly denatured species during that part of the DSC scan used for analysis (Sturtevant, 1987). Irreversible species will accumulate near the high-temperature end of each transition; therefore, to minimize errors in determining $\Delta H$ and $\Delta S$, the high-temperature end was excluded in the reversible curve fitting (Lepock et al., 1992). As expected for an irreversible transition, the DSC profiles do not fit as well with the reversible model (Figure 6C,D) because of the sharp drop in the $C_p$ above the $T_m$ of peak C. To reduce this fitting problem, peak C was fit with the high-temperature tail (beyond the peak half-height on the downslope) excluded (Figure 6C,D). Due to irreversibility, an accurate value for $\Delta C_p$ is unobtainable, so $\Delta\Delta G$ was calculated by two procedures: by assuming constant $\Delta H$ and $\Delta S$ and by estimating the temperature dependence of $\Delta H$ and $\Delta S$ using a value of 0.12 cal/g for $\Delta C_p$, which is an average value for

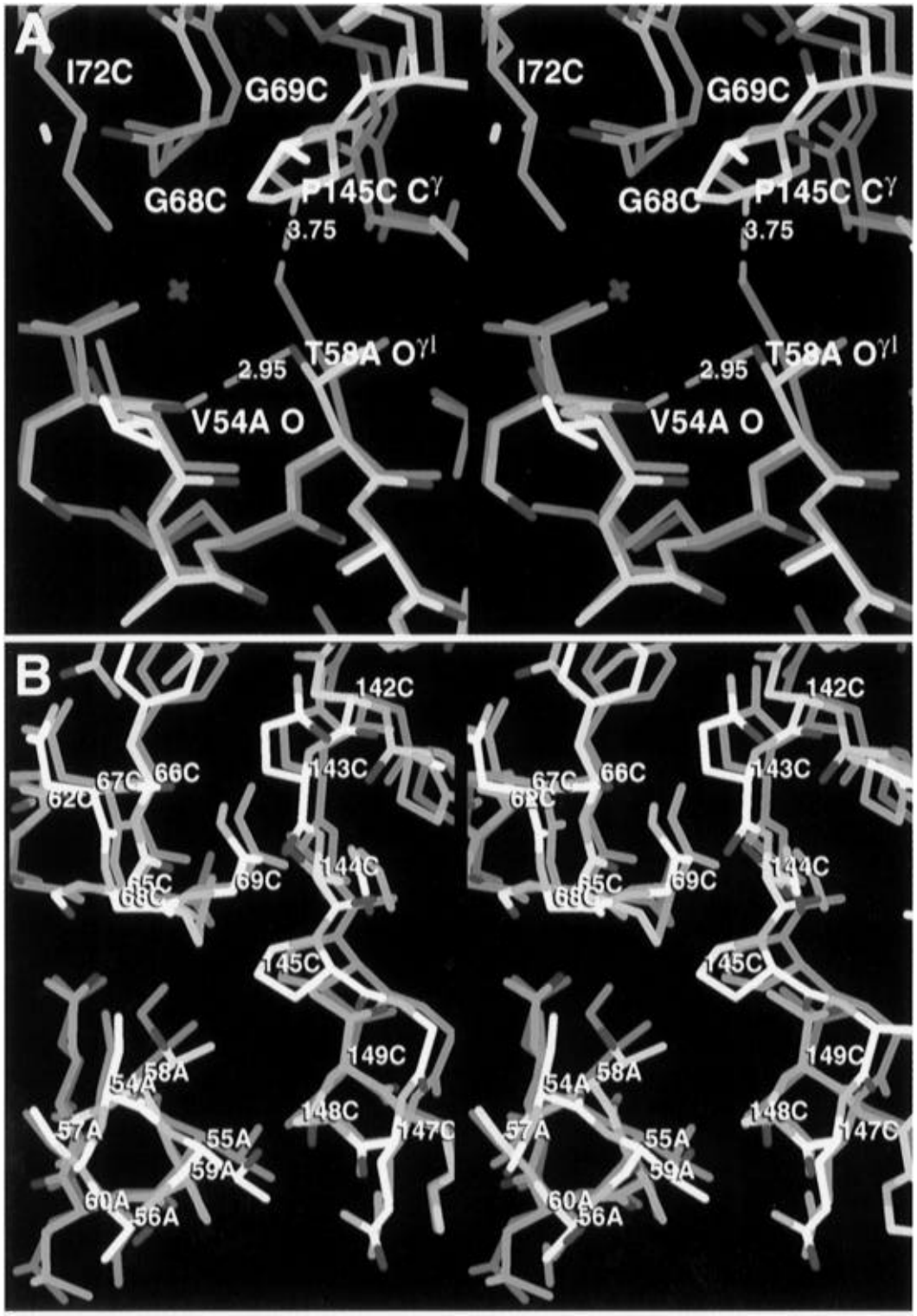


FIGURE 4: Structural consequences of the Ile58Thr mutation. Stereo diagrams comparing the native MnSOD (subunit A in green and subunit C in purple) with the Ile58Thr MnSOD structure (carbon in yellow, oxygen in red, and nitrogen in blue). The A subunits of native and mutant MnSOD were superimposed (calculation included only the main-chain atoms of the residues contributing to the tetrameric four-helix bundle interface; RMS deviation 0.3 Å). (A) Ile58 of native MnSOD contributes more packing interactions across the four-helix bundle tetrameric interface than Thr58 in the mutant Ile58Thr MnSOD. In native MnSOD, the $C^{\delta}$ of Ile58A interacts across the interface with Pro145C and main-chain atoms of 64C, 65C, and 69C. In the mutant enzyme, a hydrogen bond is formed between Thr58 $O^{\gamma 1}$ and the carbonyl oxygen of Val54 of the same subunit, and the C subunit is collapsed toward the A subunit. (B) The overall quaternary structure of the mutant Ile58Thr MnSOD is conserved, but the interface is collapsed to compensate for the loss of a methyl group. Here, the tetrameric four-helix bundle interface is viewed looking down the α2 helix that contains the Ile58Thr mutation.

several small, globular proteins (Privalov & Khechinashvili, 1974). These methods give a destabilization $\Delta\Delta G$ of 3−6 kcal/mol for transition B and 9−13 kcal/mol for transition C (Table 2).

*Thermal Inactivation*. Pulsed radiolysis measurements of activity versus temperature showed that the activity of mutant human Ile58Thr MnSOD is much more sensitive to heat than native MnSOD (Figure 7). Ile58Thr MnSOD was completely

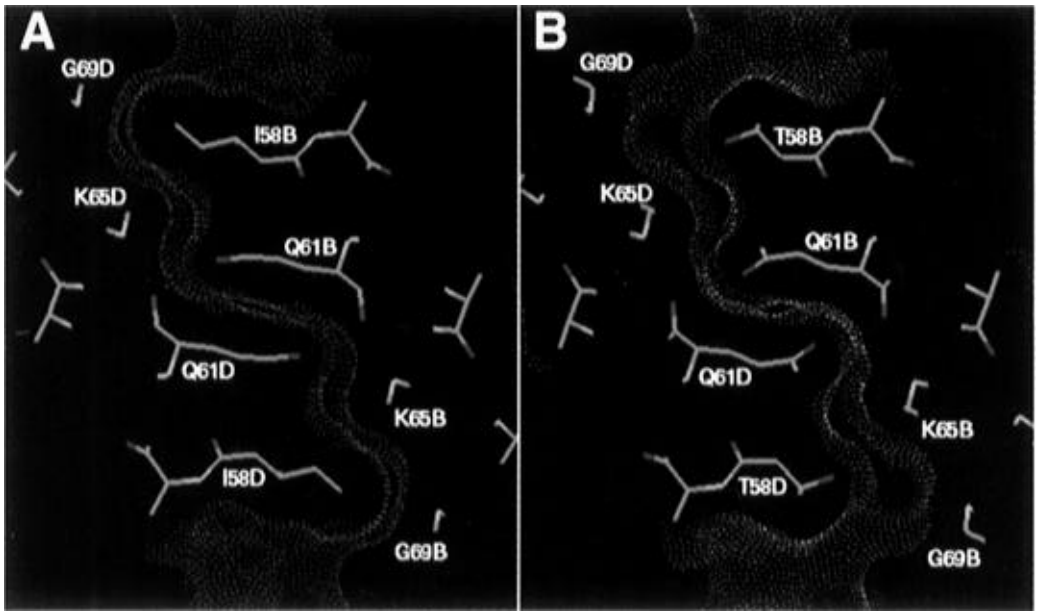


FIGURE 5: Ile58Thr MnSOD has packing defects in the mutant four-helix bundle tetrameric interface. (A) Native MnSOD molecular surface (green dots) of D (left) and B (right) subunits. Ile58B (upper right) and Ile58D (lower left) show tight shape complementarity. (B) Ile58Thr MnSOD molecular surface (yellow dots) shows gaps at Thr58B (upper right) and Thr58D (lower left). Although the mutant interface is collapsed in compensation for the mutation (see Figure 4), packing defects remain in the mutant interface that weaken the tetramer and result in a less active, temperature-sensitive enzyme. Molecular surfaces were calculated using the MS program (Connolly, 1983) with a 1.4 Å probe radius.

inactivated at 52−55 °C as compared to 72−75 °C for native human MnSOD. For native and mutant human MnSOD, the temperatures of inactivation correspond with transition B of the DSC curves (Figure 6). The mutant Ile58Thr human MnSOD is about half as active as native human MnSOD at all temperatures prior to inactivation. Interestingly, when native MnSOD is incubated for 3 h at 41.7 °C, there is almost no effect on activity, whereas mutant Ile58Thr MnSOD is completely inactivated by this treatment (data not shown; see Methods section). The inactivation predicted from DSC transition B corresponds well to the experimentally measured inactivation (see theoretical curve plotted with experimental data in Figure 7).

## DISCUSSION

*Assembly and Structure*. The Ile58Thr mutation disrupts the native tetrameric form of MnSOD and promotes a dimeric form in solution (Figure 1). Yet, Ile58Thr MnSOD has the same subunit structure as native (Figure 3A), and a native-like tetrameric form of the mutant enzyme is observed in the crystal (Figure 3B). Although the tetrameric interface surrounding Thr58 (Figure 4) has shifted in compensation for the loss of a methyl group, a cavity remains in the mutant interface (Figure 5). With two such cavities per four-helix bundle and two four-helix bundles per tetrameric interface, the final effect of the single amino acid mutation is amplified 4-fold in the MnSOD tetramer. These packing defects in the tetrameric interface disrupt the dimer−tetramer equilibrium and explain the experimental observation that the dimer is favored over the tetramer in solution (Figure 1).

*Thermal Stability and Inactivation*. For both native and Ile58Thr MnSOD, the conformational change occurring during DSC transition B is responsible for enzyme inactivation (Figures 6 and 7) and has a $\Delta T_m$ of 13.2° (Table 1). Transition C appears to be the main unfolding of the protein and has a $\Delta T_m$ of 16.5° (Table 2). Transition A is found only in the mutant MnSOD (Figure 6B; $T_m$ ∼34°), which suggests it is due to the dissociation of Ile58Thr MnSOD tetramers into dimers over a broad temperature range.

Why is Ile58Thr MnSOD so unstable relative to native enzyme? Clearly, the mutation at the tetrameric interface promotes the dissociation of the tetramer and produces a less thermostable dimeric form. For Ile58Thr MnSOD, not only is there a mutation of a buried residue in the core of the four-helix bundle, but this bundle also forms an intersubunit interface. When the tetramer disassociates into dimers, several residues normally buried in the interface are exposed and secondary structure units (e.g., the helical hairpin) are untethered. This destabilizes the overall protein fold and produces an experimentally less thermostable dimeric form.

Ile58Thr MnSOD is thermally inactivated ∼20 °C lower than native and is compromised at normal body temperatures. In the native enzyme, inactivation (Figure 7) and DSC transition B (Figure 6) occur at ∼72 °C whereas in the mutant they occur at ∼55 °C. The identity of transition B is unknown, but inactivation is clearly due to the conformational change occurring during this transition. The mutant MnSOD has predicted half-lives of only 3.2 and 1.4 h at 37 and 41 °C, as compared to 3.1 years for the native enzyme. These predictions were experimentally confirmed by the heat inactivation of mutant MnSOD by incubation for 3 h at 41.7 °C, which had no effect on native enzyme. Tetramer disassociation into dimers, especially at temperatures greater than 35 °C (Figure 6B, transition A), accounts for the extreme temperature sensitivity of the mutant. Thermal inactivation is probably due to loss of proper active site geometry and possibly even metal ion loss. The tetramer form of the enzyme is important for active site stability because the two four-helix bundles of the tetrameric interface (Figure 3B) stabilize the conformation of the helical hairpin, thereby holding two active site residues (His26 and His74, Figure 3A) in the appropriate configuration for metal ligation and

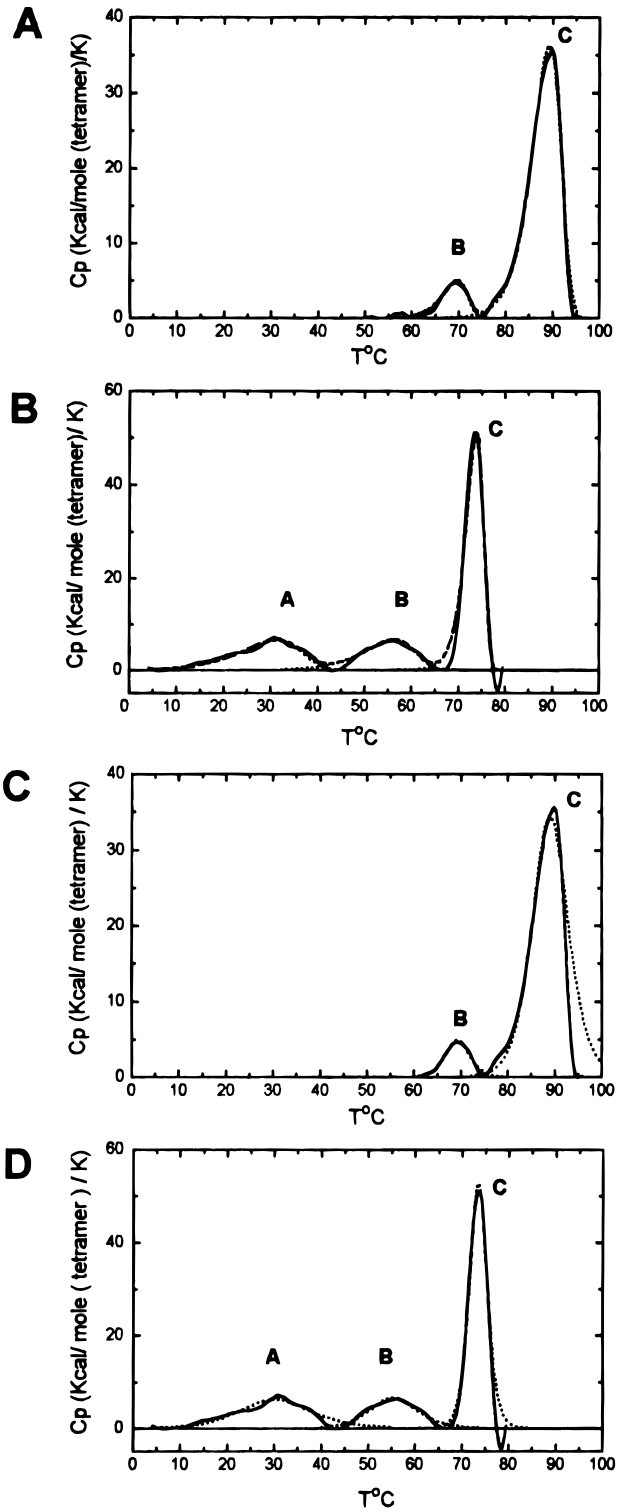


FIGURE 6: DSC profiles of apparent excess specific heat ($C_p$) vs temperature for native MnSOD (A and C) and Ile58Thr MnSOD (B and D). The dotted lines are the best fits to the individual components of the experimental profiles (solid lines). The data were fit using an irreversible model (A and B) and a reversible model (C and D) with the high-temperature tail for peak C removed (>92 °C for native and >76 °C for Ile58Thr).

activity. Tetramer disruption into dimers releases the helical hairpin, which should greatly increase its mobility and thereby disrupt the geometry of at least two of the active site ligands.

*Ile58Thr MnSOD Thermal Stability Compared to Other Proteins*. Most DSC protein stability studies focus on monomeric enzymes and report smaller $\Delta\Delta G$ and $\Delta T_m$ values than those measured for Ile58Thr MnSOD. For the main unfolding transition C, $\Delta T_m$ is 16.5 °C and $\Delta\Delta G$ is −11.2 kcal/mol of tetramer (on average, Table 2) or −2.8 kcal/mol of monomer. For example, a buried intrasubunit Cys6Ala Cu,ZnSOD mutation (McRee et al., 1990) has much smaller values ($\Delta T_m$ = 4.3 °C and $\Delta\Delta G$ = −1.3 kcal/mol of dimer or −0.65 kcal/mol of monomer) even though these mutants leave packing defects of similar size (SH for Cys6Ala and $CH_2$ for Ile58Thr). A very similar mutation, Ile3Thr, of the major hydrophobic core of T4 lysozyme (Ladbury et al., 1992) also has a much smaller $\Delta T_m$ and a comparable $\Delta\Delta G$ ($\Delta T_m$ = 8.5 °C and $\Delta\Delta G$ = −2.5 kcal/mol of monomer, pH 2.0). Eriksson and co-workers (Eriksson et al., 1992, 1993) studied several mutations of residues completely buried in the core of lysozyme. For the creation of a three-atom cavity (at Leu-46, -99, -118, -121, and -133), $\Delta T_m$ values ranged from 8.6 to 15.7 °C and $\Delta\Delta G$ values ranged from −2.7 to −5.0 kcal/mol of monomer. The Phe153Ala mutation created a 6 atom cavity with a $\Delta T_m$ of 12.3 °C and $\Delta\Delta G$ of −3.5 kcal/mol-monomer. Thus, the shift in $T_m$ and the change in $\Delta G$ caused by removing one

Table 1: Rate of Inactivation ($k_i$) and Activation Energy ($E_A$) for Transition B of MnSOD Determined by Irreversible Modeling

| enzyme | $T_m$ (°C) | $E_A$ (kcal/mol) | $k_i$ (37 °C) ($\times 10^{-7}$ s$^{-1}$) | $k_i$ (41 °C) ($\times 10^{-7}$ s$^{-1}$) |
|---|---|---|---|---|
| native | 69.2 ± 1.1 | 89.9 ± 7.7 | 0.070 ± 0.039 | 0.45 ± 0.025 |
| I58T | 56.0 ± 0.8 | 40.9 ± 2.4 | 593 ± 60 | 1370 ± 130 |

Table 2: Thermodynamic Parameters for Reversible Unfolding of MnSOD

| enzyme | component | $T_m$ (°C) | $\Delta H^a$ (kcal/mol) | $\Delta\Delta G^b$ (kcal/mol) | $\Delta\Delta G^{*c}$ (kcal/mol) |
|---|---|---|---|---|---|
| native | B | 70.0 ± 0.7 | 142.0 ± 12.0 | | |
| native | C | 88.9 ± 0.5 | 90.6 ± 6.2 | | |
| I58T | A | 34.3 ± 2.4 | 65.0 ± 25.0 | | |
| I58T | B | 56.4 ± 0.5 | 64.9 ± 1.9 | −2.7 | −6.2 |
| I58T | C | 72.4 ± 1.1 | 191.0 ± 10.0 | −9.1 | −13.2 |

[a] $\Delta H$ and $\Delta G$ are given per mole of tetramer. [b] $\Delta\Delta G$ is $\Delta G$ of the mutant calculated at the appropriate $T_m$ of the native assuming constant $\Delta H$ ($\Delta C_p$ = 0). [c] $\Delta\Delta G^*$ was calculated assuming $\Delta C_p$ = 0.12 cal/g.

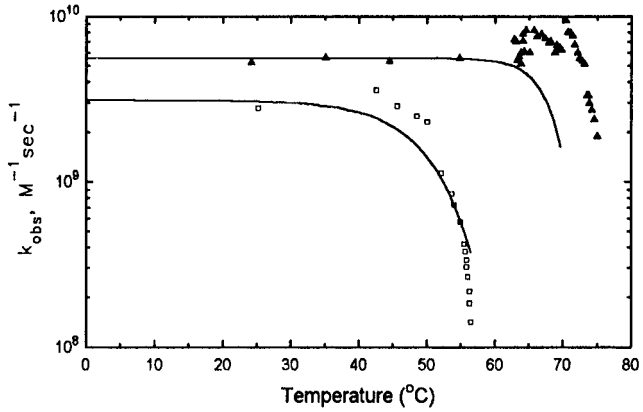


FIGURE 7: Temperature dependence of the MnSOD reaction rate measured by pulsed radiolysis. The inactivation temperature of Ile58Thr MnSOD (open squares) is ~20 °C lower than native (filled triangles). Theoretical curves (solid lines; fraction denatured ($f_D$) vs $T$; calculated by integrating eq 4 in Methods with respect to time at a specific rate of 1 °C/min, assuming that activity is directly proportional to the fraction of native protein remaining, and plotted normalized to activity measured before any inactivation) show that the DSC predicted rates (Table 1) closely match the experimental data.

carbon atom four times from the tetrameric interface of MnSOD is comparable to removing three to six carbon atoms from the core of lysozyme and accounts for the large $\Delta\Delta G$ and $\Delta T_m$ values observed with Ile58Thr MnSOD.

*Significance and Implications*. The crystal structures of defective multimeric proteins with interface point mutations that may cause an inheritable disease have rarely been analyzed in terms of their biochemical properties. A mutation at the $\alpha_1\beta_2$ interface of hemoglobin Rothschild (Trp37$\beta$Arg) destabilizes the tetramer into $\alpha_1\beta_1$ dimers (Kavanaugh et al., 1992) and causes chronic fatigue, mild anemia, and shortened red blood cell survival (Danish et al., 1982). In growth hormone receptor, a single amino acid mutation that disrupts dimer formation results in severe dwarfism and metabolic dysfunction (Duquesnoy et al., 1994), and extensive mutational analysis of hydrophobic residues in the core of the GH hormone-receptor interface has been shown to be important for interface stability (Clackson & Wells, 1995). Our mutational study of the most buried hydrophobic residue of the MnSOD tetrameric interface, Ile58, confirms the importance of hydrophobic residues in interface stability and suggests possible medical implications.

Some patients with the fatal neurodegenerative disorder familial ALS have single amino acid mutations in the dimer interface of Cu,ZnSOD (Ala4Val, Ile113Thr, Val148Gly, and Ile149Thr) that decrease SOD activity (Deng et al., 1993; Pramatarova et al., 1995). As in the four-helix bundle interface of MnSOD, the dimer interface of Cu,ZnSOD has a noncrystallographic 2-fold axis of symmetry, effectively doubling the detrimental effect of a single amino acid mutation. Here, we report a naturally occurring mutation of MnSOD that leaves four packing defects in the tetrameric interface, compromises the structural integrity of the active site, and destabilizes the enzyme as a whole. Similarly, the familial ALS Cu,ZnSOD dimer interface mutations probably produce an impaired enzyme by destabilizing the dimer interface and subsequently compromising the structural integrity of the active site and of the entire enzyme.

The decreased thermostability and tetramer assembly of the naturally occurring polymorphic variant Ile58Thr MnSOD could result in ineffective levels of this enzyme in vivo. Partly unfolded and fully unfolded proteins are thought to have higher rates of proteolytic degradation (Goldberg & St. John, 1976; Davidson et al., 1988). During illness, mutant MnSOD would also be inactivated by the elevated temperatures of fever. Unfortunately, no clinical data are available for the anonymous organ donor from whom the cDNA libraries were derived (Clonetech). Cells may compensate for Ile58Thr MnSOD by inducing MnSOD gene expression so that the basal level of MnSOD expression is higher, especially in times of stress. In human leukocytes, there is an age-dependent decline in the ability to induce MnSOD expression in response to agents which generate reactive oxygen (Niwa et al., 1993). The decline begins between the ages 45 and 55 years, and there is a dramatic loss in the ability to induce MnSOD after age 55. Thus, older people with a genetic defect in the four-helix bundle tetrameric interface of MnSOD may be especially prone to degenerative disease. A high fever could destroy their basal supply of MnSOD; recovery of basal MnSOD levels would be slowed by their reduced ability to induce MnSOD production, leaving them with a propensity for late-onset diseases.

## ACKNOWLEDGMENT

We thank Elizabeth Getzoff, Tom Terwilliger, and Susan Redford for critically reading the manuscript and Scirroco Borgstahl for useful suggestions. Pulse radiolysis rate studies were carried out at Brookhaven National Laboratory under Grant DE-AC02-76CH00016 with the U.S. Department of Energy and supported by its Division of Chemical Sciences, Office of Basic Energy Sciences.

## REFERENCES

Ames, B N., Shigenaga, M. K., & Hagen, T. M. (1993) *Proc. Natl. Acad. Sci. U.S.A. 90*, 7915−7922.
Beyer, W., Imlay, J., & Fridovich, I. (1991) *Prog. Nucleic Acid Res. Mol. Biol. 40*, 221−253.
Borgstahl, G. E. I., Parge, H. E., Hickey, M. J., Beyer, W. F., Jr., Hallewell, R. A., & Tainer, J. A. (1992) *Cell 71*, 107−118.
Brünger, A. T., Krukowski, A., & Erickson, J. W. (1990) *Acta Crystallogr., Sect. A 46*, 585−593.
Cabelli, D. E., & Bielski, B. H. (1983) *J. Phys. Chem. 87*, 1809−1812.
Carson, M. (1991) *J. Appl. Crystallogr. 24*, 958−961.
Cerutti, P. A. (1985) *Science 227*, 375−381.
Chance, B., Sies, H., & Boveris, A. (1979) *Phys. Rev. 59*, 527−605.
Church, S. L., Grant, J. W., Ridnour, L. A., Oberly, L. W., Swanson, P. E., Meltzer, P. S., & Trent, J. M. (1993) *Proc. Natl. Acad. Sci. U.S.A. 90*, 3113−3117.
Clackson, T., & Wells, J. A. (1995) *Science 267*, 383−386.
Connolly, M. L. (1983) *J. Appl. Crystallogr. 16*, 548−558.
Crouch, R. K., Gandy, S. E., Kimsey, G., Galbraith, R. A., Galbraith, G. M. P., & Buse, M. G. (1981) *Diabetes 30*, 235−241.
Danish, E. H., Harris, J. W., Ahmed, F., & Anderson, H. (1982) *Hemoglobin 6*, 51−55.
Davidson, B. L., Palella, T. D., & Kelley, W. N. (1988) *Gene 68*, 85−91.
Davies, J. L., Kawaguchi, Y., Bennett, S. T., Copeman, J. B., Cordel, H. J., Pritchard, L. E., Reed, P. W., Gough, S. C. L., Jenkins, S. C., Palmer, S. M., Balfour, K. M., Rowe, B. R., Farral, M., Barnett, A. H., Baln, S. C., & Todd, J. A. (1994) *Nature 371*, 130−136.
Deng, H.-X., Hentati, A., Tainer, J. A., Iqbal, Z., Cayabyab, A., Hung, W.-Y., Getzoff, E. D., Hu, P., Herzfeldt, B., Roos, R. P., Warner, C., Deng, G., Soriano, E., Smyth, C., Parge, H. E., Ahmed, A., Roses, A. D., Hallewell, R. A., Pericak-Vance, M. A., & Siddique, T. (1993) *Science 261*, 1047−1051.
Duquesnoy, P., Sobrier, M., Duriez, B., Dastot, F., Buchanan, C. R., Savage, M. O., Preece, M. A., Craescu, C. T., Blouquit, Y., Goossens, M., & Amselem, S. (1994) *EMBO J. 13*, 1386−1395.
Eggers, B., Kurth, J. H., & Kurth, M. C. (1994) *Am. J. Hum. Genet. 55*, A183.
Eriksson, A. E., Baase, W. A., Zhang, X. J., Heinz, D. W., Blaber, M., Baldwin, E. P., & Matthews, B. W. (1992) *Science 255*, 178−183.
Eriksson, A. E., Baase, W. A., & Matthews, B. W. (1993) *J. Mol. Biol. 229*, 747−769.
Filimonov, V. V., Potekhim, S. A., Mateev, S. W., & Privalov, P. L. (1982) *Mol. Biol. (Moscow) 16*, 551−562.
Freire, E., & Biltonen, R. L. (1978) *Biopolymers 17*, 1257−1272.
Fridovich, I. (1986) *Adv. Enzymol. 58*, 61−97.
Goldberg, A. L., & St. John, A. C. (1976) *Annu. Rev. Biochem. 45*, 747−802.
Gray, T. M., & Matthews, B. W. (1984) *J. Mol. Biol. 175*, 75−81.
Guidot, D. M., McCord, J. M., Wright, R. M., & Repine, J. E. (1993) *J. Biol. Chem. 268*, 26699−26703.
Hallewell, R. A., Masiarz, F. R., Najarian, R. C., Puma, J. P., Quiroga, M. R., Randolph, A., Sanchez-Pescador, R., Scandella, C. J., Smith, B., Steimer, K. S., & Mullenbach, G. T. (1985) *Nucleic Acids Res. 13*, 2017−2034.
Halliwell, B., & Gutteridge, J. M. C. (1989) *Free Radicals in Biology and Medicine*, Clarendon Press, Oxford.
Hjalmarsson, K., Marklund, S. L., Engström, Å., & Edlund, T. (1987) *Proc. Natl. Acad. Sci. U.S.A. 84*, 6340−6344.

Ho, Y. S., & Crapo, J. D. (1988) *FEBS Lett. 229*, 256−260.
Jones, T. A. (1985) *Methods Enzymol. 115*, 157−171.
Kavanaugh, J. S., Rogers, P. H., Case, D. A., & Arnone, A. (1992) *Biochemistry 31*, 4111−4121.
Khan, A. U., & Wilson, T. (1995) *Chem. Biol. 2*, 437−445.
Kunkel, T. A., Roberts, J. D., & Zakour, R. A. (1987) *Methods Enzymol. 154*, 367−382.
Ladbury, J. E., Hu, C. Q., & Sturtevant, J. M. (1992) *Biochemistry 31*, 10699−10702.
Lepock, J. R., Frey, H. E., & Hallewell, R. A. (1990a) *J. Biol. Chem. 265*, 21612−21618.
Lepock, J. R., Rodahl, A. M., Zhang, C., Heynen, M. L., Waters, B., & Cheng, K. H. (1990b) *Biochemistry 29*, 681−689.
Lepock, J. R., Ritchie, K. P., Kolios, M. C., Rodahl, A. M., Heinz, K., & Kruuv, J. (1992) *Biochemistry 31*, 12706−12712.
Leslie, A. G. W., Brick, P., & Wonacott, A. J. (1986) *CCP4 News 18*, 33.
Malaisse, W. J., Malaisse-Lagae, F., Sener, A., & Pipeleers, D. G. (1982) *Proc. Natl. Acad. Sci. U.S.A. 79*, 927−930.
Masuda, A., Longo, D. L., Kobayashi, Y., Appella, E., Oppenheim, J. J., & Matsushima, K. (1988) *FASEB J. 2*, 3087−3091.
McAdam, M. E., Fox, R. A., Lavelle, F., & Fielden, E. M. (1977) *Biochem. J. 165*, 71−79.
McRee, D. E. (1992) *J. Mol. Graphics 10*, 44−46.
McRee, D. E., Redford, S. M., Getzoff, E. D., Lepock, J. R., Hallewell, R. A., & Tainer, J. A. (1990) *J. Biol. Chem. 265*, 14234−14241.
Millikin, D., Meese, E., Vogelstein, B., Witkowski, C., & Trent, J. (1991) *Cancer Res. 51*, 5449−5453.
Nath, N., Chari, S. N., & Rathi, A. B. (1984) *Diabetes 33*, 586−589.
Niwa, Y., Iizawa, O., Ishimoto, K., Akamatsu, H., & Kanoh, T. (1993) *Am. J. Pathol. 143*, 312−320.
Nomikos, I. N., Wang, Y., & Lafferty, K. J. (1989) *Immunol. Cell Biol. 67*, 85−87.
Oberley, L. W., & Beuttner, G. R. (1979) *Cancer Res. 39*, 1141−1149.
Pramatarova, A., Figlewicz, D. A., Krizus, A., Han, F. Y., Ceballos-Picot, I., Nicole, A., Dib, M., Meininger, V., Brown, R. H., & Rouleau, G. A. (1995) *Am. J. Hum. Genet. 56*, 592−596.
Privalov, P. L., & Khechinashvili, N. N. (1974) *J. Mol. Chem. 86*, 665−684.
Richter, C., Park, J., & Ames, B. N. (1988) *Proc. Natl. Acad. Sci. U.S.A. 85*, 6465−6467.
Schwarz, H. A. (1981) *J. Chem. Educ. 58*, 101−105.
St. Clair, D. K., Wan, X. S., Oberley, T. D., Muse, K. E., & Clair, W. H. S. (1992) *Mol. Carcinog. 6*, 238−242.
Sturtevant, J. M. (1987) *Annu. Rev. Phys. Chem. 38*, 463−488.
Sun, Y. (1990) *Free Radical Biol. Med. 8*, 583−599.
Sun, Y., Colburn, N. H., & Oberley, L. W. (1993) *Oncol. Res. 5*, 127−132.
Trent, J. M., Stanbridge, E. J., McBride, H. L., Meese, E. U., Casey, G., Araujo, D. E., Witkowski, C. M., & Nagle, R. B. (1990) *Science 247*, 568−571.
Winterbourn, C. C. (1993) *Free. Radical Biol. Med. 14*, 85−90.
Wispe, J. R., Clark, J. C., Burhans, M. S., Kropp, K. E., Korfhagen, T. R., & Whitsett, J. A. (1989) *Biochim. Biophys. Acta 994*, 30−36.
Wong, G. H. W., & Goeddel, D. V. (1988) *Science 242*, 941−943.
Wong, G. H., Elwell, J. H., Oberley, L. W., & Goeddel, D. V. (1989) *Cell 58*, 923−931.
Yahara, O., Hashimoto, K., Taniguchi, N., Ishikawa, M., Sato, Y., Yamashita, H., & Ohno, H. (1991) *Res. Commun. Chem. Pathol. Pharmacol. 72*, 315−326.

BI951892W